A HIGHER-ORDER ROBERT-ASSELIN TYPE TIME FILTER

YONG LI[*] AND CATALIN TRENCHEA[†]

Abstract. The Robert-Asselin (RA) time filter combined with leapfrog scheme is widely used in numerical models of weather and climate. It successfully suppresses the spurious computational mode associated with the leapfrog method, but it also weakly dampens the physical mode and degrades the numerical accuracy. The Robert-Asselin-Williams (RAW) time filter is a modification of the RA filter that reduces the undesired numerical damping of RA filter and increases the accuracy. We propose a higher-order RA (hoRA) type time filter which effectively suppresses the computational modes and achieves *third-order* accuracy with the same storage requirement as RAW filter. Like RA and RAW filters, the hoRA filter is non-intrusive, and so it would be easily implementable. The leapfrog scheme with hoRA filter is almost as accurate, stable and efficient as the intrusive third-order Adams-Bashforth (AB3) method.

1. Introduction. The leapfrog scheme applied to the ordinary differential equation

$$u'(t) = f(u) \tag{1.1}$$

is given by

$$u^{n+1} - u^{n-1} = 2\Delta t f(u^n),$$

where Δt denotes the time step and u^n denotes the numerical solution approximating the exact solution u at time $t^n = n\Delta t$. The leapfrog scheme (also known as the midpoint rule or the explicit Nyström method) is an explicit second-order neutral time-stepping method. It is best suited for the integration of linear oscillation systems, and is widely used in weather and climate computational models (see [1] and references therein). The weakness of the leapfrog scheme is its undamped computational mode, the so-called "time splitting" instability [2, 3, 1].

One way to avoid the problem with the leapfrog scheme's computational mode is by using a different explicit time-stepping scheme, e.g., the second-order Adams-Bashforth method [4], the third-order Adams-Bashforth method [2], the leapfrog-trapezoidal method [5, 6] or the Magazenkov method [7]. Another way is by non-intrusively post-processing the leapfrog scheme based legacy codes. The non-intrusive RA time filter designed by Robert [8] and analyzed by Asselin [9] successfully suppresses the computational mode. Currently, the RA filter is used in operational numerical weather prediction models, atmospheric general circulation models for climate simulation, ocean general circulation models, models of the fluids in rotating annulus laboratory experiments, etc. (see [1] for more details). However, the RA time filter also weakly suppresses the physical mode, and hence it degrades the numerical accuracy − reducing the $\mathcal{O}(\Delta t^2)$ truncation error of the unfiltered leapfrog scheme to $\mathcal{O}(\Delta t)$.

Williams [1] introduced an important modification to the RA filter − the RAW time filter (see also [10]). When used in conjunction with the leapfrog scheme, the RAW filter increases the accuracy to almost second-order truncation error. The behavior of the RAW filter was analyzed in semi-implicit integrations [11] and also in the Simplified Parameterizations, Primitive Equation Dynamics atmospheric general circulation model [12]. In [13], Williams proposed two slightly intrusive schemes with increased storage requirements which provide higher-order accuracy for the amplitude of the physical mode.

We propose a higher-order Robert-Asselin (hoRA) type time filter, a non-intrusive linear post process to the leapfrog scheme, aiming to resolve the issue with the computational mode as well as increase numerical accuracy. The hoRA-filtered leapfrog scheme applied to (1.1) is given by

$$v^{n+1} = u^{n-1} + 2\Delta t f(v^n),$$

---
[*]Department of Mathematics, 301 Thackeray Hall, University of Pittsburgh, Pittsburgh, PA 15260, Email: yol34@pitt.edu

[†]Department of Mathematics, 301 Thackeray Hall, University of Pittsburgh, Pittsburgh, PA 15260, Email: trenchea@pitt.edu

$$u^n = v^n + \frac{\beta}{2}(v^{n+1} - 2v^n + u^{n-1}) - \frac{\beta}{2}(v^n - 2u^{n-1} + u^{n-2}),$$

where the dimensionless parameter β is in the interval $[0, 1)$. Here v and u denote the unfiltered and once-filtered values, respectively. The hoRA filter improves the $\mathcal{O}(\Delta t)$ truncation error of RA to at least $\mathcal{O}(\Delta t^2)$. In particular, when the parameter $\beta = 0.4$, the truncation error (2.4) becomes *third* order, yielding $\mathcal{O}(\Delta t^4)$ amplitude and phase-speed errors for the physical mode (see formulae (2.6) and (2.7)). Also in this case, the computational modes of hoRA-filtered leapfrog scheme are strongly damped (see Figure 2.2). The storage factor[*] for leapfrog scheme combined with hoRA filters is 4 (see Table 2.2). Compared with the intrusive AB3 method, the hoRA-filtered leapfrog scheme is almost as accurate, stable and efficient, yet non-intrusive and easily implementable in existing legacy codes. Thus, the leapfrog scheme with hoRA filter is suitable to simulate the long-time behavior of weather and climate models.

The paper is organized as follows. The hoRA time filter is described and analyzed in Section 2, where its theoretical properties are compared with RA, RAW and AB3. Section 3 presents several numerical tests comparing the performance of leapfrog scheme combined with RA, RAW and hoRA filters as well as the AB3 method. The conclusions appear in Section 4.

2. Linear analysis.

2.1. The RA and RAW time filters. The amplitude and phase-speed errors of time-stepping schemes for non-dissipative dynamical systems may be examined by analyzing solutions to the oscillation equation (see e.g., [2, 3] and references therein)

$$\frac{du}{dt} = i\omega u, \tag{2.1}$$

where ω is a real constant. Throughout the text, we will denote the time step as Δt, the exact solution u at time $t^n = n\Delta t$ as $u(t^n)$, and the numerical solution approximating $u(t^n)$ as u^n.

The RAW-filtered leapfrog (LF) scheme (LF-RAW) applied to (2.1) is given by

$$w^{n+1} = u^{n-1} + 2i\omega\Delta t\, v^n, \tag{LF}$$

$$u^n = v^n + \frac{\nu\alpha}{2}(w^{n+1} - 2v^n + u^{n-1}), \tag{RA}$$

$$v^{n+1} = w^{n+1} + \frac{\nu(\alpha - 1)}{2}(w^{n+1} - 2v^n + u^{n-1}), \tag{W}$$

where the dimensionless parameter ν is usually $\mathcal{O}(0.01 - 0.2)$ and the parameter α is typically around 0.5. Here w, v and u denote, respectively, the unfiltered, once-filtered and twice-filtered values. When $\alpha = 1$ the (W) step drops out and LF-RAW recovers to LF-RA, and when $\nu = 0$ the leapfrog scheme is recovered.

Both RA and RAW filters successfully dampen the computational mode associated with leapfrog scheme. Compared with RA filter, however, the RAW filter provides higher accuracy for the amplitude of the physical mode (see Table 2.2). More precisely, the amplitude error for the physical mode of LF-RAW is second-order accurate for $\alpha \in (0.5, 1]$, and of particular interest, it is fourth-order accurate when $\alpha = 0.5$ in which case the three-time-level mean is conserved [1]. However, LF-RAW is unconditionally unstable in this case [14]. Thus, Williams suggests taking $\alpha \gtrapprox 0.5$, e.g., $\alpha = 0.53$ to obtain almost fourth-order accuracy for the amplitude of the physical mode [1].

2.2. The higher-order Robert-Asselin type time filter. The leapfrog scheme with hoRA time filter (LF-hoRA) applied to (2.1) is given by

$$v^{n+1} = u^{n-1} + 2i\omega\Delta t\, v^n, \tag{LF}$$

---

[*]The storage factor is the number of full arrays that must be allocated for each unknown variables in order to implement each scheme [2].

$$u^n = v^n + \frac{\beta}{2}(v^{n+1} - 2v^n + u^{n-1}) - \frac{\beta}{2}(v^n - 2u^{n-1} + u^{n-2}), \qquad \text{(hoRA)}$$

where the dimensionless parameter β is in the interval $(0, 1)$.[†‡] Here v and u denote the unfiltered and once-filtered values, respectively. In the limit of good time resolution, i.e., $\omega\Delta t \ll 1$, the LF-hoRA scheme provides higher-order accuracy for the amplitude and phase speed of the physical mode (see (2.6) and (2.7)).

Eliminating v^{n+1} in (LF) and (hoRA) gives

$$v^n = \frac{u^n - 2\beta u^{n-1} + \frac{\beta}{2} u^{n-2}}{1 - \frac{3}{2}\beta + i\beta\omega\Delta t},$$

and hence

$$v^{n+1} = \frac{u^{n+1} - 2\beta u^n + \frac{\beta}{2} u^{n-1}}{1 - \frac{3}{2}\beta + i\beta\omega\Delta t}.$$

Substituting v^n and v^{n+1} in (hoRA) gives an equivalent formula to the LF-hoRA scheme:

$$u^{n+1} - 2\beta u^n - (1 - 2\beta)u^{n-1} = i\omega\Delta t(2u^n - 3\beta u^{n-1} + \beta u^{n-2}). \qquad (2.2)$$

Thus, the amplification factor, $A = u^{n+1}/u^n$, for LF-hoRA satisfies the following cubic equation.

$$A^3 - 2(\beta + i\omega\Delta t)A^2 + (3\beta i\omega\Delta t - 1 + 2\beta)A - \beta i\omega\Delta t = 0. \qquad (2.3)$$

The equation (2.3) has three roots with one physical mode, denoted by A_+, and two computational modes. The exact solution to (2.1) is $u(t) = u(0)\exp(i\omega t)$ and the exact amplification factor is $A_{\text{exact}} = \exp(i\omega\Delta t)$.

The exact and the numerical amplification factors for LF-hoRA scheme in the complex plane are plotted in Figure 2.1. The exact amplification factor lies on the unit circle as $\omega\Delta t$ increases from 0 to 1. Like AB3 method [2], the physical mode of LF-hoRA stays inside the unit circle, while one computational mode becomes amplified when $\omega\Delta t$ exceeds $\sqrt{\frac{3}{4} + \beta - \beta^2}/(1 + \frac{3}{2}\beta - \beta^2)$ (see (2.5) in Section 2.4).
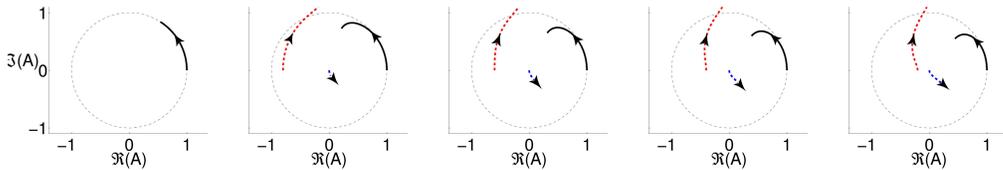

Fig. 2.1: Amplification factors plotted in the complex plane. From left to right: exact amplification factor, numerical amplification factors for LF-hoRA scheme with $\beta = 0.1$, 0.2, 0.3 and 0.4, respectively. Solid line is the physical mode and two dashed curves represent computational modes.

Magnitudes of numerical amplification factors for the LF-hoRA scheme are shown in Figure 2.2. Both computational modes are effectively controlled by the hoRA filter, especially when $\beta = 0.4$.

[†]Since the LF-hoRA scheme recovers to leapfrog method when $\beta = 0$, we assume $\beta \neq 0$ throughout the text.

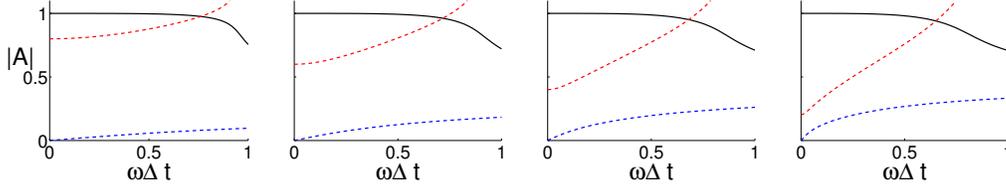[‡]The computational mode of LF-hoRA scheme is amplified if $\beta < 0$ or $\beta \geq 1$.

Fig. 2.2: Magnitudes of amplification factors for LF-hoRA scheme, plotted as functions of $\omega\Delta t$. From left to right: $\beta = 0.1, 0.2, 0.3$ and 0.4, respectively. Solid line is the physical mode and two dashed curves represent computational modes.

2.3. The consistency order of LF-hoRA. By Taylor expansion of $u(t^{n+1})$, $u(t^{n-1})$ and $u(t^{n-2})$ at time t^n, the truncation error of LF-hoRA from (2.2) is

$$
\begin{aligned}
\tau_n(\Delta t) = & \frac{u(t^{n+1}) - 2\beta u(t^n) - (1-2\beta)u(t^{n-1})}{\Delta t} \\
& - i\omega(2u(t^n) - 3\beta u(t^{n-1}) + \beta u(t^{n-2})) \\
= & \frac{2-5\beta}{6}(i\omega\Delta t)^2 u'(t^n) + \frac{11\beta}{12}(i\omega\Delta t)^3 u'(t^n) + \mathcal{O}[(i\omega\Delta t)^4].
\end{aligned}
\tag{2.4}
$$

Thus, the LF-hoRA scheme is of order 3 when $\beta = 0.4$[§] and of order 2 otherwise.

2.4. The stability domain of LF-hoRA. To determine the maximum $\omega\Delta t$ for which all numerical amplification factors of the LF-hoRA scheme are non-amplified, we follow the *root locus curve* method (see e.g., [15]). The characteristic equation of (2.2) is

$$
\zeta^3 - 2\beta\zeta^2 - (1-2\beta)\zeta - z(2\zeta^2 - 3\beta\zeta + \beta) = 0,
$$

where ζ denotes the points on the unit circle, i.e., $\zeta = e^{i\theta}$ for $\theta \in [0, 2\pi]$, and $z \in \mathbb{C}$. The curve z is called the *root locus curve*. In our case $z = i\omega\Delta t$ lies on the imaginary axis, and consequently, θ satisfies

$$
\cos\theta = 1 \ \text{ or } \ \cos\theta = \beta - \frac{1}{2},
$$

and

$$
z = 0 \ \text{ or } \ z = \pm i\frac{\sqrt{\frac{3}{4} + \beta - \beta^2}}{1 + \frac{3}{2}\beta - \beta^2},
$$

which indicate the intersections of the root locus curve with imaginary axis in the complex z-plane. Thus, the stability of the LF-hoRA scheme is provided by

$$
\omega\Delta t \leq \frac{\sqrt{\frac{3}{4} + \beta - \beta^2}}{1 + \frac{3}{2}\beta - \beta^2}, \ \ 0 < \beta < 1.
\tag{2.5}
$$

Several root locus curves for various values of β are plotted in Figure 2.3.

[§]The choice $\beta = 0.4 + \mathcal{O}(\omega\Delta t)$ also preserves the higher consistency error of $\beta = 0.4$.
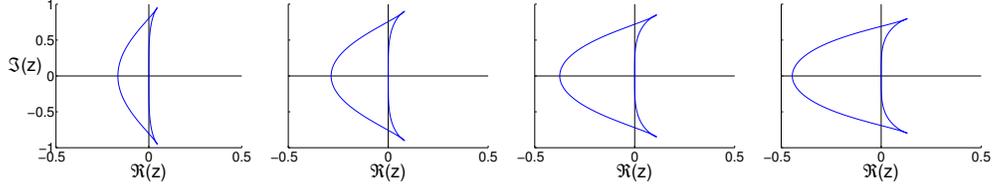
Fig. 2.3: Root locus curves of LF-hoRA scheme. From left to right: $\beta = 0.1,\ 0.2,\ 0.3$ and 0.4, respectively. The stability of LF-hoRA scheme is given by the intersection of the root locus curve with the imaginary axis.

2.5. Error analysis for amplitude and phase speed of the physical mode for LF-hoRA scheme. The first few terms in the Taylor expansion $A_+ = \sum\limits_{n=0}^{\infty} a_n(\beta)(i\omega\Delta t)^n$ for the physical mode of LF-hoRA scheme are[¶]

$$a_0 = 1,\ a_1 = 1,\ a_2 = \frac{1}{2},\ a_3 = \frac{\beta}{4(1-\beta)}, \text{ and } a_4 = -\frac{1}{8} - \frac{\beta}{8(1-\beta)^2}.$$

The amplitude for the physical mode of LF-hoRA scheme is fourth-order accurate:

$$|A_+| - |A_{\text{exact}}| = |A_+| - 1 = \frac{\beta(2\beta - 3)}{8(1-\beta)^2}(\omega\Delta t)^4 + \mathcal{O}[(\omega\Delta t)^6],\ \beta \in (0,1). \tag{2.6}$$

Figure 2.4 compares magnitudes of the physical mode for various values of β. Note that the amplitude error grows as β increases.

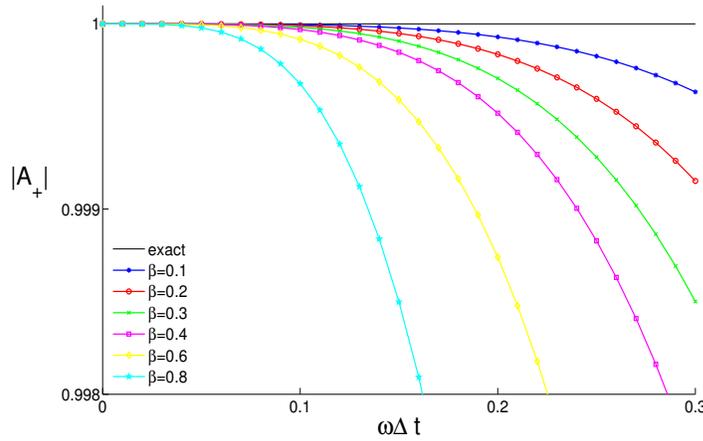Fig. 2.4: Magnitudes of the physical mode for LF-hoRA scheme, plotted as functions of $\omega\Delta t$.

The phase-speed error of the physical mode for LF-hoRA scheme is given by

$$R_+ - 1 = \frac{\arg(A_+)}{\arg(A_{\text{exact}})} - 1 = \frac{2 - 5\beta}{12(1-\beta)}(\omega\Delta t)^2 + O[(\omega\Delta t)^4],\ \beta \in (0,1), \tag{2.7}$$

[¶]The coefficients of the Taylor expansion are obtained using symbolic manipulation of Mathematica.

where $R_+ = \arg(A_+)/\arg(A_{\text{exact}})$ denotes the relative phase change in the physical mode. The phase speed of the physical mode is fourth-order accurate when $\beta = 0.4$ and second-order accurate otherwise. Figure 2.5 shows relative phase changes in the physical modes. The phase-speed error decays as β increases from 0 to 0.4, and then grows as β increases afterwards.
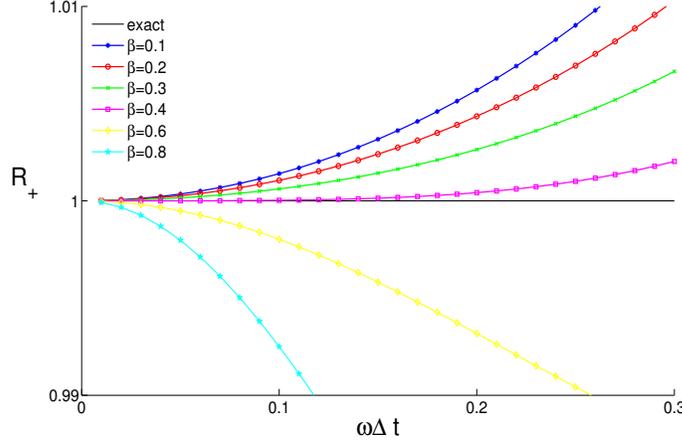

Fig. 2.5: Relative phase changes in the physical mode for LF-hoRA scheme, plotted as functions of $\omega\Delta t$.

Table 2.1 summarizes a few properties of amplitude and phase-speed errors for the physical mode of LF-hoRA scheme. Since both amplitude and phase-speed errors increase when $\beta > 0.4$, we narrow down the choice of β within the interval $(0, 0.4]$, and especially the case $\beta = 0.4$ in order to obtain higher-order accuracy.

	$\beta \in (0, 0.4]$	$\beta \in (0.4, 1)$	Order of accuracy
Amplitude error	↗	↗	4th
Phase-speed error	↘	↗	4th at $\beta = 0.4$, otherwise 2nd

Table 2.1: Changes in amplitude and phase-speed errors for the physical mode of LF-hoRA scheme as β varies. The notation ↗ and ↘ indicate the increase and decrease in the errors as β grows, respectively.

2.6. Comparison of RA, RAW and hoRA filters. In Figure 2.6, we compare magnitudes of the physical modes for LF-RA, LF-RAW and LF-hoRA schemes. We choose the RA-parameter $\nu = 0.2$ and RAW-parameters $\alpha = 0.53$, $\nu = 0.2$. The amplitude of LF-hoRA scheme is fourth order, while the both amplitudes of LF-RA and LF-RAW schemes are only second order (see Table 2.2).

Figure 2.7 compares the relative phase changes in the physical modes. Note that the phase-speed error of the LF-hoRA scheme for $\beta = 0.4$ is significantly smaller than the phase-speed errors of both LF-RA and LF-RAW.

2.7. Comparison of LF-hoRA and AB3 schemes. The third-order LF-hoRA scheme ($\beta = 0.4$) has the following properties:

(i) It follows from (2.4) that the truncation error is

$$\tau_n(\Delta t) = \frac{11}{30}(i\omega\Delta t)^3 u'(t^n) + \mathcal{O}[(i\omega\Delta t)^4].$$

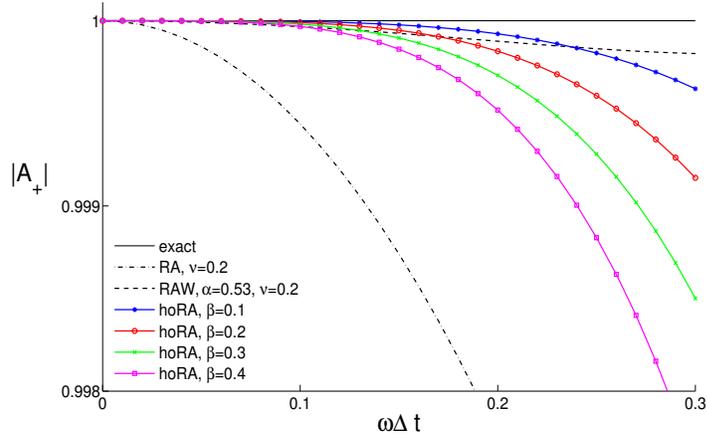(ii) By (2.5), the LF-hoRA scheme is stable for $\omega\Delta t \leq 0.69$.

6

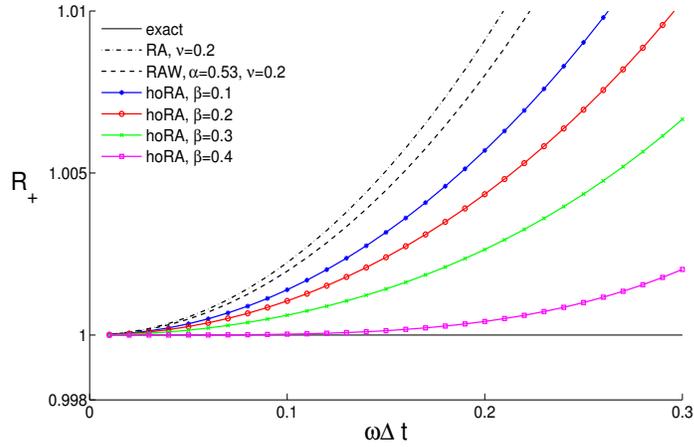Fig. 2.6: Magnitudes of the physical modes, plotted as functions of $\omega\Delta t$.

Fig. 2.7: Relative phase changes in the physical modes, plotted as functions of $\omega\Delta t$.

(iii) The scheme requires one new function evaluation per time step.

Recall that the *efficiency factor* is defined as the maximum stable time step with which the oscillation equation can be integrated, divided by the number of function evaluations per time step [2]. It follows from (ii) and (iii) that the efficiency factor of LF-hoRA scheme is 0.69.

On the other hand, the AB3 method applied to (1.1)

$$u^{n+1} = u^n + \frac{\Delta t}{12}\left(23f(u^n) - 16f(u^{n-1}) + 5f(u^{n-2})\right),$$

has the following properties [2]:

(i) the truncation error is

$$\tau_n(\Delta t) = \frac{3}{8}(i\omega\Delta t)^3 u'(t^n) + \mathcal{O}[(i\omega\Delta t)^4],$$

7

(ii) the method is stable for $\omega\Delta t \leq 0.72$,

(iii) it also requires one new function evaluation in each time step.

The efficiency factor of AB3 method is 0.72. Thus, the LF-hoRA scheme is almost as accurate, stable and efficient as the intrusive AB3 method.

As in [2], a few properties of several time-stepping methods are summarized in Table 2.2.

Method	Order	Strg. factors	Amplitude Error	Phase-speed error	Max. $\omega\Delta t$
Leapfrog	2	2	1	$1+\frac{(\omega\Delta t)^2}{6}$	1
LF-RA	1	3	$1-\frac{\nu}{2(2-\nu)}(\omega\Delta t)^2$	$1+\frac{1+\nu}{3(2-\nu)}(\omega\Delta t)^2$	$\sqrt{\frac{2-\nu}{2+\nu}}$
LF-RAW	1 or 2	4	$1+\frac{\nu(1-2\alpha)}{2(2-\nu)}(\omega\Delta t)^2$	$1+\left(\frac{(1-\nu(1-\alpha))(2-\alpha\nu)}{(2-\nu)^2}-\frac{1}{3}\right)(\omega\Delta t)^2$	$r(\alpha,\nu)$
LF-hoRA	2 or 3	4	$1+\frac{\beta(2\beta-3)}{8(1-\beta)^2}(\omega\Delta t)^4$	$1+\frac{2-5\beta}{12(1-\beta)}(\omega\Delta t)^2+\mathcal{O}(\omega\Delta t)^4$	$\sqrt{\frac{\frac{3}{4}+\beta-\beta^2}{1+\frac{3}{2}\beta-\beta^2}}$
LF-hoRA ($\beta=0.4$)	3	4	$1-0.306(\omega\Delta t)^4$	$1+0.024(\omega\Delta t)^4$	0.69
AB3	3	4	$1-0.375(\omega\Delta t)^4$	$1+0.401(\omega\Delta t)^4$	0.72

Table 2.2: Comparison of time-stepping schemes. The explicit form of $r(\alpha,\nu)$ [14] is given by $r(\alpha,\nu)=\sqrt{\frac{(2\alpha-1)(2-\nu)}{\alpha^2(2+\nu(2\alpha-1))}}$.

3. Numerical tests. In this section we perform several numerical tests on the leapfrog scheme with RA, RAW and hoRA filters, and on the AB3 method. These tests verify the advantages of hoRA filter in various aspects. Section 3.1 shows that the hoRA filter preserves both amplitude and phase with high accuracy. In Section 3.2, the hoRA filter is shown to effectively control the computational modes. Section 3.3 shows that the LF-hoRA scheme captures the physics of a model with reasonable fidelity.

3.1. Simple pendulum. Consider a simple pendulum problem, which is given by two coupled non-linear equations (also see [13]):

$$\frac{d\theta}{dt} = v/L,$$
$$\frac{dv}{dt} = -g\sin\theta,$$

where θ, v, L and g denote, respectively, angular displacement, velocity along the arc, length of the pendulum, and the acceleration due to gravity. Set $g=9.8$ and $L=49$ to easily observe the long time behavior of numerical solutions. We choose the initial condition $(\theta_0, v_0) = (0.9\pi, 0)$ at $t=0$ and the time step $\Delta t = 0.1$, and then numerically integrate the system using LF-RA ($\nu=0.2$), LF-RAW ($\alpha=0.53$, $\nu=0.2$) and LF-hoRA ($\beta=0.4$) schemes over the time interval $[0, 200]$. The Runge-Kutta (RK) 4 method is used to initialize the second step of each scheme and also for the third step of LF-hoRA. Then compare the corresponding results with the reference solution, which is computed using the adaptive RK4(5) method with relative error tolerance 10^{-10} and absolute error tolerance 10^{-15}.

The comparison is shown in Figure 3.1. The phase errors of LF-RA scheme are considerably large, and the amplitudes decrease relatively fast. Although both RAW and hoRA filters preserve the amplitudes highly accurately, the LF-hoRA solutions stay much closer to the reference solutions due to its fourth-order accuracy in the phase speed.

3.2. Lorenz system. Consider the Lorenz system:

$$\frac{dX}{dt} = \sigma(Y-X),$$
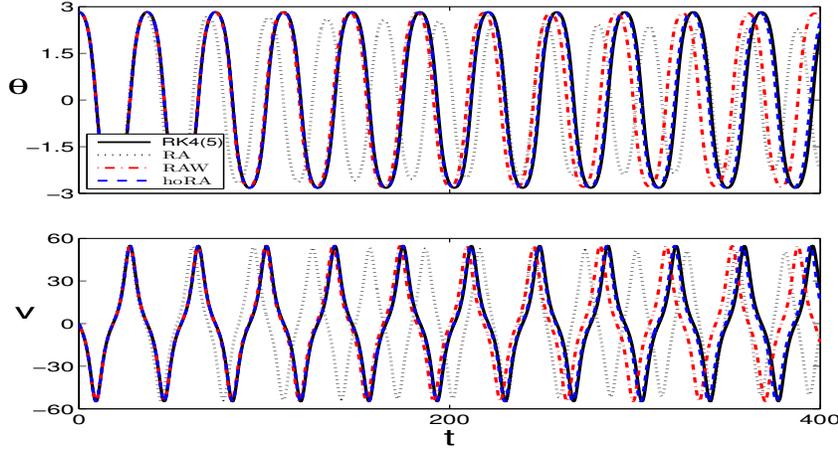$$\frac{dY}{dt} = -XZ+rX-Y,$$
$$\frac{dZ}{dt} = XY-bZ.$$

Fig. 3.1: Numerical solutions to the simple pendulum, computed by LF-RA ($\nu = 0.2$), LF-RAW ($\alpha = 0.53$, $\nu = 0.2$) and LF-hoRA ($\beta = 0.4$) schemes, are compared with the reference solutions obtained from adaptive RK4(5) method with relative error tolerance 10^{-10} and absolute error tolerance 10^{-15}. The initial condition is $(\theta_0, v_0) = (0.9\pi, 0)$ at $t = 0$ and the time step is $\Delta t = 0.1$.

As in [2], we choose $\sigma = 12$, $r = 12$, $b = 6$, and the initial condition $(X_0, Y_0, Z_0) = (-10, -10, 25)$ at $t = 0$. The system is numerically integrated over the time interval $[0, 1.5]$ using LF-RA, LF-RAW, LF-hoRA and AB3 schemes, with time step $\Delta t = 0.016$ and all other filter-parameters exactly the same as in the previous test. Again, the reference solution is computed using the adaptive RK4(5) method with the same error tolerances as before.

The numerical solutions for X are plotted in Figure 3.2 (the reference solution is almost overlapped by LF-hoRA solution). The solutions of LF-RA and LF-RAW start oscillate from $t = 0.75$ and produce large errors. The solutions of LF-hoRA and AB3, on the other hand, are significantly more accurate and do not oscillate due to their third-order accuracy and the excellent control on the computational modes, respectively.[||]

3.3. Ozone Photochemistry. Consider an example of reactions between atomic oxygen (O), nitrogen oxides (NO and NO$_2$), and ozone (O$_3$) (see [3] for more details):

$$NO_2 + h\nu \xrightarrow{k_1} NO + O,$$

$$O + O_2 \xrightarrow{k_2} O_3,$$

$$NO + O_3 \xrightarrow{k_3} O_2 + NO_2,$$
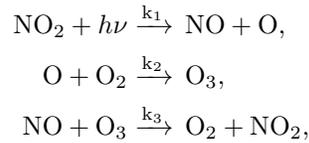
where $h\nu$ denotes a photon of solar radiation. Let $c = (c_1, c_2, c_3, c_4)$ represent the concentration in molecules per cubic centimeter of O, NO, NO$_2$ and O$_3$, respectively. Assuming that the background concentration of O$_2$ is constant, the reactions are governed by the following system:

$$\frac{dc_1}{dt} = k_1 c_3 - k_2 c_1,$$

$$\frac{dc_2}{dt} = k_1 c_3 - k_3 c_2 c_4,$$

$$\frac{dc_3}{dt} = k_3 c_2 c_4 - k_1 c_3,$$

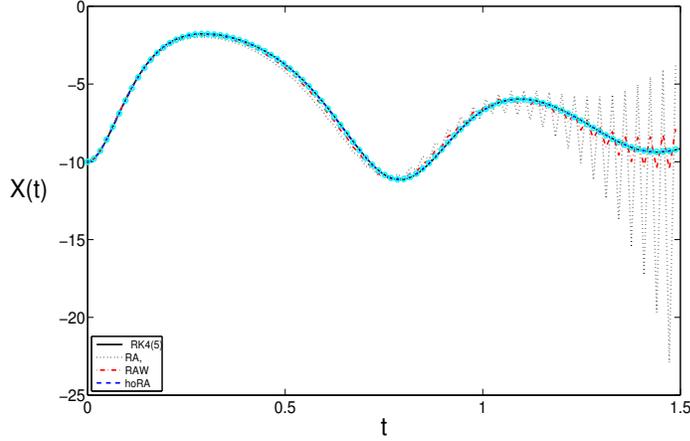[||] See Figure 1 in [2] for the computational modes of AB3 method.

9

Fig. 3.2: Numerical solutions to Lorenz system for variable X, computed by LF-RA ($\nu = 0.2$), LF-RAW ($\alpha = 0.53$, $\nu = 0.2$), LF-hoRA ($\beta = 0.4$) and AB3 schemes, are compared with the reference solution obtained from the adaptive RK4(5) method with relative error tolerance 10^{-10} and absolute error tolerance 10^{-15}. The initial condition is $(X_0, Y_0, Z_0) = (-10, -10, 25)$ at $t = 0$ and the time step is $\Delta t = 0.016$.

$$\frac{dc_4}{dt} = k_2 c_1 - k_3 c_2 c_4.$$

Here

$$k_1 = 10^{-2} \max\{0, \sin(2\pi t/t_d)\} \text{s}^{-1},$$

$$k_2 = 10^{-2} \text{s}^{-1}, {}^{**} \ k_3 = 10^{-16} \text{cm}^3 \text{molecule}^{-1} \text{s}^{-1},$$

where t_d is the length of 1 day in seconds. With initial condition $c_0 = (0, 0, 5 \times 10^{11}, 8 \times 10^{11})$ molecules cm^{-3} at $t = 0$, the reference solution is computed using the adaptive RK4(5) method with same error tolerances as before, and the numerical solution is computed using LF-hoRA scheme for $\beta = 0.4$ and time step $\Delta t = 40$ s. The chemical concentrations over the next 2 days are shown in Figure 3.3. With the fixed time step, the LF-hoRA scheme is able to capture the behavior of the concentrations with reasonable accuracy.

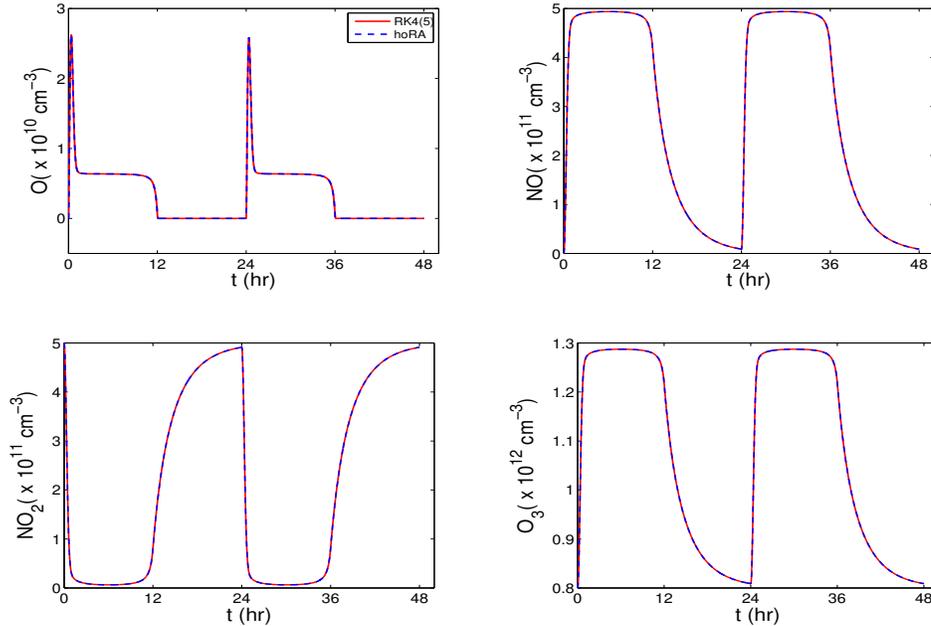**We choose $k_2 = 10^{-2}$ instead of 10^5 as in [3], to make the reaction equations non-stiff.

Fig. 3.3: Numerical solutions for chemical concentrations, computed using LF-hoRA scheme with $\beta = 0.4$, are compared with the reference solutions obtained from adaptive RK4(5) method with relative error tolerance 10^{-10} and absolute error tolerance 10^{-15}. The initial condition is $c_0 = (0, 0, 5 \times 10^{11}, 8 \times 10^{11})$ molecules cm^{-3} at $t = 0$, and the time step is $\Delta t = 40$ s.

4. Conclusions. We proposed and analyzed a higher-order Robert-Asselin type time filter. With the same storage requirement as RAW filter, hoRA increases the numerical accuracy to *third* order. The hoRA filter is an efficient, accurate post process which effectively controls the computational modes. Thus, the LF-hoRA scheme is suitable to simulate the long-time behavior of weather and climate models. In addition, the hoRA filter is non-intrusive and easily implementable in existing legacy codes.

REFERENCES

[1] P. D. Williams, A Proposed Modification to the Robert-Asselin Time Filter, Monthly Weather Review 137 (8) (2009) 2538–2546.
doi:10.1175/2009MWR2724.1. 1, 2

[2] D. R. Durran, The Third-Order Adams-Bashforth Method: An Attractive Alternative to Leapfrog Time Differencing, Monthly Weather Review 119 (3) (1991) 702–720.
doi:10.1175/1520-0493(1991)119<0702:TTOABM>2.0.CO;2. 1, 2, 3, 7, 8, 9

[3] D. R. Durran, Numerical methods for fluid dynamics, 2nd Edition, Vol. 32 of Texts in Applied Mathematics, Springer, New York, 2010, with applications to geophysics.
doi:10.1007/978-1-4419-6412-0. 1, 2, 9, 10

[4] D. Lilly, On the computational stability of numerical solutions of time-dependent non-linear geophysical fluid dynamics problems, Monthly Weather Review 93 (1) (1965) 11–25.
doi:10.1175/1520-0493(1965)093<0011:OTCSON>2.3.CO;2. 1

[5] Y. Kurihara, On the Use of Implicit and Iterative Methods for the Time Integration of the Wave Equation, Monthly Weather Review 93 (1) (1965) 33–46.
doi:10.1175/1520-0493(1965)093<0033:OTUOIA>2.3.CO;2. 1

[6] S. Zalesak, Fully multidimensional flux-corrected transport algorithms for fluids, Journal of computational physics 31 (3) (1979) 335–362.
doi:10.1016/0021-9991(79)90051-2. 1

[7] L. Magazenkov, Trudy Glavnoi Geofizicheskoi Observatorii, (Transactions of the Main Geophysical Observatory) 410 (1980) 120:129. 1

[8] A. J. Robert, The integration of a low order spectral form of the primitive meteorological equations, Journal of the Meteorological Society of Japan 44, Ser. 2 (5) (1966) 237–245. 1

[9] R. Asselin, Frequency filter for time integrations, Monthly Weather Review 100 (6) (1972) 487–490.
doi:10.1175/1520-0493(1972)100<0487:FFFTI>2.3.CO;2. 1

[10] R. J. Smith, Minimizing time-stepping errors in numerical models of the atmosphere and ocean, Master's thesis, University of Reading (2010). 1

[11] P. D. Williams, The RAW filter: An improvement to the Robert–Asselin filter in semi-implicit integrations, Monthly Weather Review 139 (6) (2011) 1996–2007.
doi:10.1175/2010MWR3601.1. 1

[12] J. Amezcua, E. Kalnay, P. D. Williams, The effects of the RAW filter on the climatology and forecast skill of the SPEEDY model, Monthly Weather Review 139 (2) (2011) 608–619.
doi:10.1175/2010MWR3530.1. 1

[13] P. D. Williams, Achieving seventh-order amplitude accuracy in leapfrog integrations, Monthly Weather Review (2013), in press.
doi:10.1175/MWR-D-12-00303.1. 1, 8

[14] N. Hurl, W. Layton, Y. Li, C. Trenchea, Stability analysis of the Crank-Nicolson-Leap-Frog method with the Robert-Asselin-Williams time filter, submitted.
URL http://www.mathematics.pitt.edu/sites/default/files/research-pdfs/CNLFraw.pdf 2, 8

[15] E. Hairer, G. Wanner, Solving ordinary differential equations. II, Vol. 14 of Springer Series in Computational Mathematics, Springer-Verlag, Berlin, 2010, stiff and differential-algebraic problems, Second revised edition.
doi:10.1007/978-3-642-05221-7. 4